Integrated Rehabilitation Of Corrosion-Damaged RC Beams: Enhancing Flexural Capacity And Failure Predictability With Grout And Externally Bonded GFRP

Jasman Yusuf[1*] and Achmad Zultan Mansur[2]

[1] Civil Engineering Department of Muhammadiyah Parepare University, Parepare, 91131, Indonesia.
[2] Civil Engineering Department of Borneo Tarakan University, Tarakan, 77123, Indonesia.
[*] Corresponding author. E-mail: jasmanyusuf70@gmail.com

Received: Mar. 29, 2026; Accepted: Jul. 11, 2026

Corrosion-induced deterioration in reinforced concrete structures poses a critical threat to structural integrity and service life. This study investigates the effectiveness of an integrated rehabilitation strategy that combines geometric restoration using highstrength, non-shrink grout (Sikagrout 215) with flexural strengthening via externally bonded glass fiber-reinforced polymer (GFRP) composites on beams damaged by simulated corrosion-induced section loss and spalling. An experimental program was conducted on two groups: unstrengthened control beams (NB) and rehabilitated specimens (GFB). Key performance indicators, including ultimate load capacity, loaddeflection response, concrete and steel strain development, and GFRP strain evolution, were systematically analyzed. Results demonstrate that GFRP-strengthened beams achieved a 10.87% higher average ultimate load (34.64 kN) than sound control beams (31.24 kN). Although the GFRP layer resulted in a slightly lower ultimate concrete strain in GFB (2391 $\mu\varepsilon$) compared to NB (2821 $\mu\varepsilon$), the rehabilitated beams exhibited enhanced structural resilience, evidenced by a 28.82% increase in yield load and a 25.08% reduction in mid-span deflection at ultimate failure. Furthermore, the failure mode shifted from conventional ductile flexural failure in control beams to a highly predictable GFRP rupture, without premature shear failure. GFRP strain measurements confirmed full material utilization, with recorded rupture strains of $15,672$ and $18,532$ $\mu\varepsilon$ aligning within an 8% margin of theoretical predictions. These findings validate that the proposed dual-phase rehabilitation approach recovers lost strength while quantitatively enhancing structural resilience and failure predictability, offering a practical, evidence-based solution for extending the service life of aging infrastructure affected by corrosion.

Keywords: Integrated Rehabilitation, GFRP, Corrosion, RC Beams, Flexural Capacity, Ductility

http://dx.doi.org/10.6180/jase.202611_34.006

1. Introduction

Corrosion-induced deterioration remains one of the most critical threats to the durability and service life of aging reinforced concrete (RC) infrastructure worldwide. The expansion of corrosion products directly causes concrete cracking and spalling, significantly reducing the effective cross-section of reinforcement bars and the ultimate load-carrying capacity of structural members [1, 2]. This degradation, often accelerated by aggressive environmental conditions, leads to the loss of composite action between concrete and steel, potentially resulting in catastrophic failure if left untreated [3]. Therefore, developing effective, predictable, and sustainable rehabilitation methods is essential for maintaining structural safety and extending the service life of infrastructure [4].

The application of externally bonded Fiber-Reinforced Polymer (FRP) composites has become a dominant and highly effective method for strengthening deteriorated reinforced concrete (RC) structures [5, 6]. Glass Fiber Reinforced Polymer (GFRP) sheets, in particular, provide a practical, lightweight, and corrosion-resistant solution for restoring and enhancing the flexural capacity of damaged concrete beams [7, 8]. However, the success of FRP systems in real-world applications depends heavily on the condition of the concrete substrate [9]. Existing experimental studies often use laboratory specimens prepared under controlled, ideal surface conditions and employ simulated corrosion methods (e.g., accelerated electrocorrosion), which typically produce uniform and artificially induced damage [10, 11]. This conventional approach fails to replicate the heterogeneity and complexity of actual field conditions, which include uneven spalling, porous and degraded concrete surface textures, and significantly poor bond conditions between the old concrete and new repair materials [12]. This discrepancy creates a critical knowledge gap: the structural performance of an integrated rehabilitation system-combining geometric restoration (using grout) and flexural strengthening (using GFRP)-on beams with realistic, non-uniform field damage remains poorly understood [13]. A successful rehabilitation strategy requires validating the effectiveness of the composite action when interface integrity is severely compromised, a topic that has not been comprehensively addressed in the current literature [14, 15].

In this context, an 'Integrated Rehabilitation' strategy is defined as a holistic repair sequence involving two distinct stages: (1) chemical-physical compatibility through geometric restoration using high-strength, non-shrink grout (Sikagrout 215) to replace spalled concrete, and (2) structural enhancement via externally bonded GFRP wrapping. The mechanistic novelty of this integrated rehabilitation design lies in the dual-phase synergistic interaction between the high-strength non-shrink grout matrix and the externally bonded GFRP composite, operating as a unified structural system. Mechanically, the application of Sikagrout 215 transcends mere cosmetic patching of the spalled concrete cover; it structurally restores the geometric integrity of the cross-section. This geometric restoration provides a continuous, highly rigid, and dimensionally stable substrate that critically prevents localized stress concentrations. Consequently, it creates an optimal interfacial plane for the subsequently bonded GFRP sheets. Conversely, the high-tensile GFRP outer wrap plays a dual protective and structural role. It suppresses macroscopic crack propagation and diffuses shear-slip stresses within the interface transition zone (ITZ). Furthermore, the GFRP envelope exerts a passive confinement pressure over the rehabilitated tension zone. This continuous confinement restrains the lateral expansion of the newly cast grout under heavy flexural loading, effectively postponing premature micro-cracking and spalling of the repair patch. This interdependent stress-transfer mechanism fundamentally ensures that the ultimate capacity of the composite system is governed by predictable material rupture rather than premature debonding or substrate delamination. Driven by this mechanistic concept, this study aims to evaluate the overall structural effectiveness and failure behavior of this integrated rehabilitation strategy on large-scale reinforced concrete (RC) beams exhibiting simulated field damage, such as spalling and reinforcement section loss. This objective is achieved by systematically analyzing key performance indicators, including ultimate load capacity, load-deflection response, concrete and steel strain development, and failure mode transitions. The primary scientific contribution of this research is to provide practical, evidence-based design guidelines, ensuring a reliable and performance-driven solution for the sustainable rehabilitation of deteriorated concrete structures under realistic operational conditions.

2. Materials and methods

Specimen Design and Fabrication

This study employs an experimental approach to evaluate the rehabilitation performance of reinforced concrete blocks subjected to corrosion-induced spalling. Six full-scale (1:1) reinforced concrete blocks were fabricated at the Materials and Structures Laboratory, Department of Civil Engineering, Hasanuddin University. All specimens have identical dimensions of 150 mm (width) $\times$200 mm (height) $\times$3300 mm (length), with a net span of 3000 mm. The specimens are divided into two groups (see Fig. 1):

- Control beam (NB): three beams with intact reinforcement.
- Rehabilitation beams (GFB): three beams with simulated cross-sectional loss caused by corrosion and spalling, subsequently repaired and reinforced.

The concrete mixture was designed to achieve a target 28-day compressive strength of $f'c = 25$MPa with a water-cement ratio of 0.48 . The mix proportions per cubic meter included 360 kg of Type I Portland cement (52.5 MPa), 720 kg of fine aggregate, 1080 kg of coarse aggregate (maximum size 20 mm), and 173 kg of mixing water, following the guidelines for normal-weight concrete provided by ACI Committee 211 (2019). The reinforcement configuration comprised: (i) top reinforcement of 2∅8 mm plain steel bars; (ii) stirrups of ∅8 mm plain steel spaced at 150 mm ; and (iii) bottom reinforcement of either 2∅13 mm

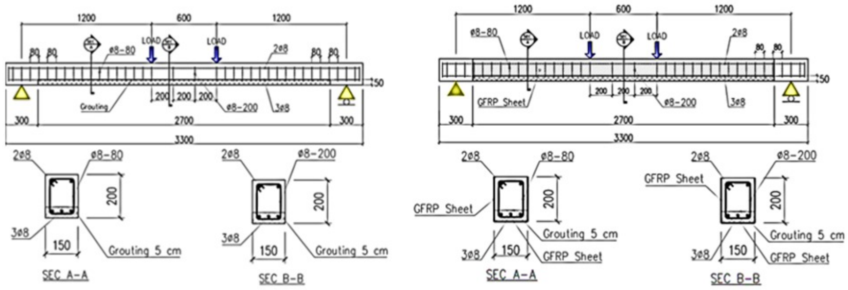

(a) Control beam. (b) Variation beam GFB.

Fig. 1. Specimen Detail.

deformed steel bars (for NB specimens) or 3∅8 mm plain steel bars (for GFB specimens) to simulate cross-sectional loss associated with early-stage steel degradation. Tensile test results confirmed average yield strengths of 378.9 MPa for ∅8 mm plain bars and 325.2 MPa for ∅13 mm deformed bars, consistent with ASTM International (2023) requirements.

To realistically represent the structural degradation caused by reinforcement corrosion and concrete spalling, the GFB specimens underwent a controlled mechanical simulation process. This method was chosen over accelerated electrochemical corrosion to ensure a precise, repeatable, and uniform reduction in the reinforcement cross-section across all samples within practical laboratory durations [10, 11]. The simulation was conducted in three sequential steps:

Step 1: Mechanical Section Loss Simulation. The standard tensile reinforcement used in the sound control beams (2∅13 mm deformed bars) was replaced in the GFB specimens with 3∅8 mm plain steel bars. This substitution resulted in a calculated reduction of the steel crosssectional area, effectively simulating the equivalent deterioration level of approximately 10% section loss, representing early-to-moderate corrosion damage where flexural stiffness reduction becomes structurally significant [2,3].

Step 2: Simulated Concrete Spalling (Intentional Uncasting). During the casting of the GFB specimens, a 50 mm high portion of the beam's soffit (bottom tension zone) was intentionally left uncast over the entire length of the span. This created a physical void (Fig. 2a-b), exposing the 3∅8 mm bars and replicating the loss of concrete cover, localized pitting, cracking, and bond degradation commonly observed in deteriorated bridge girders [10, 11]. Similar controlled deterioration approaches have been widely adopted in experimental studies to investigate the structural implications of reinforcement degradation without requiring prolonged natural exposure periods (ACI Committee 440, 2015; ISIS Canada, 2020; Melchers et al., 2006 [10]; Coronelli and Gambarova, 2004 [11]).

Step 3: Atmospheric pre-oxidation. After casting, the exposed 3∅8 mm steel bars were subjected to natural atmospheric conditions for 14 days. This allowed for the formation of a surface oxide layer (rust) on the bars, ensuring that the interface between the steel and the subsequent repair material (Sikagrout 215) would realistically mimic the surface condition of actual corroded reinforcement.

Although accelerated corrosion methods may produce different rust morphology compared to long-term natural corrosion [2, 10, 11], the adopted mechanical methodology remains appropriate for evaluating the structural rehabilitation effectiveness of the proposed grout-GFRP system. This approach is consistent with previous investigations on hybrid steelFRP strengthening systems, where controlled section loss was considered sufficient to assess flexural rehabilitation performance [16, 17]. Nevertheless, future studies incorporating naturally corroded specimens or long-term environmental exposure are recommended to further validate the proposed strategy under realistic field conditions [6, 18].

3. Rehabilitation materials and implementation procedures

3.1. Concrete Repair with Sikagrout 215

At 21 days of age, the spalled surface of the GFB specimen was repaired using Sikagrout 215 (Sika Indonesia), a high-strength, non-shrink cement grout. Before application, the concrete surface was mechanically cleaned with a wire brush and compressed air to remove loose particles and rust. The grout was mixed with water at a ratio of 0.14 : 1 by weight using a high-speed mixer for 3 minutes until homogeneous, then manually applied to restore the full cross-sectional height of 200 mm (Fig. 2c). Sikagrout 215 was specifically selected for its superior interfacial bonding characteristics; its microstructure is engineered to provide high early strength and negligible shrinkage. This ensures that the Interface Transition Zone (ITZ) between the repair grout and the existing concrete remains monolithic under flexural loading. Such micro-mechanical interlocking is crucial for preventing delamination at the interface before the GFRP layers reach their ultimate capacity. Finally, the curing process was conducted for 7 days by covering the surface with a wet sack to prevent plastic shrinkage cracking.

3.2. Reinforcement with GFRP

At 28 days of age, the repaired beams were externally reinforced using the Tyfo® Fiberwrap Composite System SEH-51A (Fyfe Company, USA), a unidirectional glass fiber-reinforced polymer (GFRP) sheet bonded with epoxy resin. The reinforcement was applied to the bottom and both sides, excluding the top side (Figure 1b; Figures 2d-e).

The GFRP installation procedure follows the wet-layup method per the manufacturer's recommendations and international standards for concrete structure reinforcement. Before application, the concrete surface is sanded to achieve a Concrete Surface Profile (CSP) of at least 3, ensuring optimal mechanical bonding between the concrete and the composite system. Dust and loose particles are then thoroughly removed using compressed air. Once the surface is clean and dry, a primer layer of Tyfo® S resin is applied evenly as a penetration layer. Subsequently, two layers of Tyfo® SEH-51A sheets (each 0.33 mm thick) are placed on the primed surface, with additional resin applied between the layers to ensure full fiber impregnation. Trapped air bubbles are removed using a pressurized rubber roller to achieve homogeneous resin distribution and maximize adhesion between the layers. After installation, a final protective layer of Tyfo® S resin is applied to prevent degradation from exposure to UV rays and environmental moisture. The complete specifications of the materials used in this procedure are summarized in Table 1.

3.3. Testing and Measurement Instruments

Four-point bending tests were conducted at 35 days of age using a 500 kN hydraulic actuator (Fig. 3). The beams were placed on two simple supports with a net span of 3000 mm. Two centralized loads were applied symmetrically, each positioned 1000 mm from the nearest support, creating a constant moment zone 1000 mm long at the center of the span (ASTM C78/C78M-21, ASTM International).

The monotonic loading was applied at a displacement-controlled rate of 0.5 mm/min, consistent with quasi-static testing protocols for structural concrete elements (PCI Handbook, 2017). Instrumentation included a load cell ($\pm 0.5\%$ accuracy), a midspan LVDT (100 mm capacity, 0.01 mm resolution), and 120Ω strain gauges bonded to tensile reinforcement and GFRP surfaces, following ACI 440.3R recommendations. Data were acquired at 1 kN intervals during elastic response and at 0.1 kN increments near critical events (cracking, yielding, and peak load), in accordance with ASTM E2309. Visual observations of crack patterns, widths, and failure mechanisms are continuously conducted.

To evaluate the deformation characteristics of the tested beams, a deformation capacity index was assessed based on the ratio between ultimate deflection and yield deflection ($\mu_\Delta = \Delta_u / \Delta_y$), where Δ_u represents the midspan deflection at ultimate load and Δ_y corresponds to the deflection at steel yielding. It should be noted that, for GFRP-strengthened members, this parameter does not represent classical material ductility as defined for yielding steel systems, since GFRP behaves predominantly as a linear-elastic brittle material up to rupture. Therefore, the calculated index in the present study is interpreted as an indicator of post-yield deformation capacity or pseudo-ductile structural behavior rather than conventional ductility [5, 7].

4. Results dan discussions

4.1. Bending Capacity of Reinforced Concrete Beams

The reduction of tensile reinforcement from deformed D13 bars to plain ∅8 bars results in a 52% loss of structural capacity due to concrete spalling, leaving the beam only 48% of its original strength. This significant degradation necessitates structural intervention to restore serviceability and ensure compliance with safety standards. An experimental evaluation was conducted across three critical performance stages: cracking, steel yielding, and ultimate load. These stages provide essential insights into the structural behavior of reinforced concrete beams under progressive damage. The cracking stage marks the onset of tensile failure and informs serviceability limits. The yielding stage reflects ductility and post-cracking reserve capacity [18]. The ultimate stage quantifies the maximum load-bearing capacity prior to Table 2 collapse. These parameters are fundamental to the performance-based assessment of structural integrity, as outlined by Johnson and Eswari (2025) [19].

The efficacy of externally bonded fibre-reinforced polymer (FRP) systems in restoring and enhancing the flexural capacity of damaged concrete members has been consistently demonstrated in the literature. Studies such as Khan and Starr (2022) reported that carbon FRP strengthening of spalled beams recovered lost strength, improved stiffness, and delayed yielding. Furthermore, Karzad *et al*. (2019) confirmed that GFRP retrofitting significantly en-

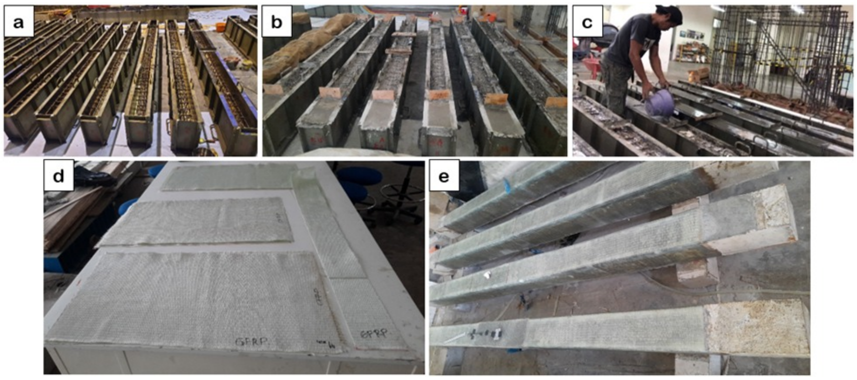

Fig. 2. Fabrication of test materials.

Table 1. Properties of Materials Used.

Material	Parameter	Value	Standard
Concrete	Fc′ (28 days)	25 MPa	ASTM C39
Plain steel bars ∅8 mm	Fy	378.90 MPa	ASTM A615
Threaded steel ∅13 mm	Fy	325.15 MPa	ASTM A615
Sikagrout 215	Compressive strength	$\geq$ 55MPa	ASTM C109
	Modulus of elasticity	$\geq$ 25GPa	ASTM C469
Tyfo® SEH-51A	Tensile strength	1034 MPa	ASTM D3039
	Modulus of elasticity	42 GPa	ASTM D3039
	The Last Resort	2.50%	-
Resin Tyfo® S	Shear Strength (Lap Shear)	$\geq$ 18MPa	ASTM D1002

Table 2. Experimental Load and Moment Capacities at Critical Stages for Unstrengthened and GFRP-Strengthened Beams.

	Test Results					
Specimens	Mcrack (kN.m)	Pcrack (kN)	Myield (kN.m)	Pyield (kN)	Multimate (kN.m)	Pultimate (kN)
NB-01	4.34	4.90	18.01	27.68	19.17	29.62
NB-02	3.86	4.09	18.98	29.29	20.57	31.95
NB-03	3.41	3.35	16.49	25.15	20.69	32.15
Average	**3.87**	**4.11**	**17.83**	**27.37**	**20.15**	**31.24**
GFB-01	6.62	8.03	16.05	23.75	23.61	36.35
GFB-02	7.90	10.16	16.18	23.96	22.02	33.69
GFB-03	8.42	11.03	16.46	24.42	22.14	33.89
Average	**7.65**	**9.74**	**16.23**	**24.04**	**22.59**	**34.64**

hances the ultimate load capacity and ductility of beams with degraded reinforcement. These established findings strongly align with the present experimental results. Test data presented in Table 2 clearly demonstrate that the GFRP-strengthened beams not only recover their lost structural capacity but also exceed the capacity of the original, unstrengthened control beams. The results show that the average ultimate moment and load increased from 20.15 kNm and 31.24 kN (unstrengthened NB specimens) to 22.59 kN•m and 34.64 kN (GFRP-strengthened GFB specimens), representing a gain in ultimate load capacity. This finding confirms that GFRP retrofitting is highly effective in mitigating strength loss caused by concrete spalling and further enhances the load-carrying capacity beyond baseline conditions [17, 20]. Thus, this integrated approach offers a viable and efficient solution for rehabilitating deteriorated concrete structures in practical engineering applications.

While the integrated rehabilitation approach shows high efficacy under laboratory conditions, the long-term durability of the epoxy bond remains a critical factor for practical infrastructure applications. Environmental stressors, such as hygrothermal aging and thermal cycling, can potentially degrade the interfacial bond between the GFRP and concrete substrate over time. Future research should focus on the performance of this integrated system under sustained environmental loading to ensure its reliability in various

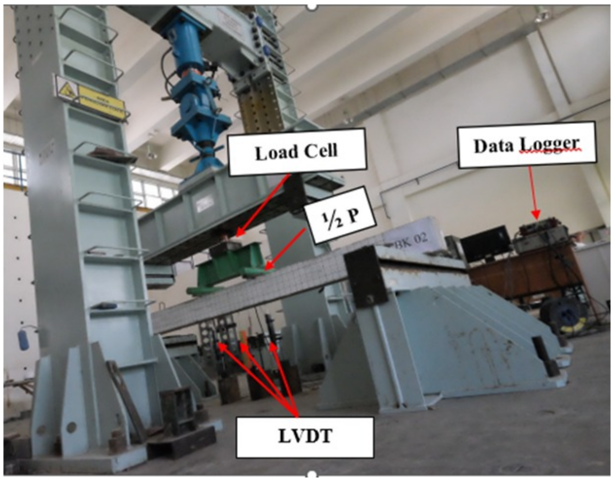

Fig. 3. Four-Point Bending Testing Scheme and Instrumentation System.

climatic conditions.

4.2. Deformation and Strain at Critical Stages

The deformation behavior and strain response of materials are essential indicators for evaluating the capacity and ductility of reinforced concrete structures, particularly after degradation such as spalling or reinforcement loss. Understanding the relationship between load, deflection, and strain in steel and concrete is crucial for analyzing safety and failure mechanisms.

This study analyzed experimental data from six beam specimens: three control beams (NB) and three GFRP-reinforced beams (GFB). The analysis aims to investigate the influence of composite reinforcement on the evolution of deformation and strain distribution under monotonic loading. We focus on three critical stages: yielding, melting, and ultimate. The comparison between the control beam group (NB) and the reinforced beam group (GFB) in Table 3 reveals significant changes in the strain response of steel (εs)) and concrete (εc), as well as an increase in deflection capacity at failure.

4.3. Load vs Deflection Behavior

The increased structural rigidity of GFB beams compared to control beams (NB) was confirmed by analyzing the load-deflection curve (Fig. 4) and the numerical data in Table 2.

In the early stages of loading, the slope of the GFB curve is steeper, indicating that the GFRP reinforcement system enhances the effective stiffness of the cross-section. This observation aligns with the findings of Mensah et al. (2020) [21], who reported that the mechanical bond between GFRP and concrete improves local stress distribution and reduces

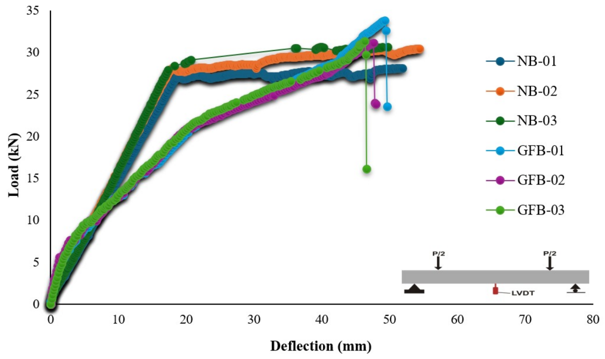

Fig. 4. Relationship between NB and GFB beam deflection.

initial inelastic deformation. The trilinear response pattern of the GFB curve reflects a smooth transition from the elastic to elastoplastic phase and ultimately to failure, indicating that the GFRP sheet inhibits crack propagation and prolongs the post-yielding phase. These findings are consistent with Fergani et al. (2018) [22], who demonstrated that GFRP reinforcement in corroded beams significantly delays the degradation of rigidity.

Quantitatively, the structural efficacy of the integrated rehabilitation strategy is evidenced by the distinct deformational and capacity transitions between the specimen groups. The average yield deflection of the GFRP-strengthened beams (GFB) reached 22.30 mm, marking a 20.8% increase over the control beams (NB), which exhibited an average yield deflection of 18.45 mm. This extended deformational capacity occurred despite the GFB specimens exhibiting a slightly lower average yielding load (24.04 kN) compared to the NB beams (27.37 kN). Crucially, this post-yielding response should not be misconstrued as classical elastoplastic ductility, given that the GFRP laminate maintains a strictly linear-elastic behavior until rupture. Instead, this structural characteristic is more precisely categorized as pseudo-ductility, defined by an extended deformation envelope prior to ultimate collapse [17, 22]. To mathematically quantify this deformational behavior, the structural ductility of the control beams and the pseudo-ductility of the rehabilitated system were evaluated using the displacement-based ductility index ($\mu = \Delta u/\Delta y$), where Δu and Δy represent the ultimate and yield deflections, respectively. The control beams (NB) exhibited a conventional ductility index of 2.14, derived from an ultimate deflection (Δu) of 39.50 mm . In comparison, despite the elastic-brittle nature of the external composite, the GFB specimens successfully maintained a robust, closely matched pseudo-ductility index of 2.16 , driven by a significantly expanded ultimate deflection (Δu) of 48.20 mm.

This geometrically extended index provides conclusive

Table 3. Deformation and Strain at Critical Stages for Unstrengthened and GFRP Strengthened Beams .

Specimens	Yield				Ultimate			
	Load (kN)	Deflection (mm)	εs yield (μe)	εc yield (μe)	Load (kN)	Deflection (mm)	εs ultimate (μe)	εc ultimate (μe)
NB-01	27.68	18.64	2011	1204	29.62	52.56	2071	2071
NB-02	29.29	21.22	1627	1329	31.95	57.08	3282	3287
NB-03	25.15	15.5	1680	945	32.15	51.82	3088	3097
Average	**27.37**	**18.45**	**1772.67**	**1159.33**	**31.24**	**53.82**	**2813.67**	**2818.33**
GFB-01	23.75	22,14	1556	1016	36,35	49,64	2181	2185
GFB-02	23.96	22,22	1753	1000	33,69	48,24	2443	2498
GFB-03	24.42	22,54	2086	1129	33,89	46,73	2487	2490
Average	**24.04**	**22.30**	**1798.33**	**1048.33**	**34.64**	**48.20**	**2370.33**	**2391.00**

mathematical proof that the integrated Sikagrout-GFRP system does not induce a catastrophic, sudden brittle failure postyielding. Instead, the substantial simultaneous increases in both yield and ultimate deflections expand the total energy dissipation capacity under the load-deflection envelope. This deformation response culminated in an average ultimate load capacity of 34.64 kN for the GFB group, representing a 10.87% increase relative to the sound control beams (31.24 kN). Interestingly, this capacity enhancement was achieved even though the ultimate concrete strain of the GFB specimens ($2391 \mu\varepsilon$) was lower than that of the NB beams ($2821 \mu\varepsilon$). Rather than indicating premature failure, this lower concrete strain signifies a highly stabilized and controlled damage progression, providing improved post-yield structural resilience that aligns with the mechanisms documented by Dang et al. [23], where fiber composites delay localized concrete crushing through confinement and active stress redistribution. Mechanically, this interaction confirms that the composite action successfully preserves an adequate structural warning capacity, characterized by progressive concrete cracking and visible major deflections prior to ultimate fiber rupture, thereby satisfying critical structural safety and serviceability requirements.

This superior flexural performance and capacity recovery provide definitive empirical validation for the systemic synergy developed between the non-shrink repair grout and the externally bonded GFRP laminate. This optimized behavior cannot be attributed to either material in isolation, but is a direct manifestation of their coupled mechanical response. The high compressive strength ($\geq$ 55MPa) and negligible shrinkage characteristics of Sikagrout 215 established a monolithic interface transition zone (ITZ) with the old concrete substrate via micro-mechanical interlocking. By precisely re-establishing the original cross-sectional height of 200 mm , the grout matrix effectively repositioned the externally bonded GFRP sheet at the extreme tension fiber, thereby maximizing the internal lever arm ($\surd$) of the reinforced section. During the post-yielding stage, as macro-tensile cracks initiated within the repair zone, the bonded GFRP sheet successfully intercepted these crack tips. This action redistributed localized stresses across the cracked planes via interfacial shear transfer through the epoxy matrix, thereby minimizing stress concentrations that typically induce premature delamination in poorly prepared substrates. Concurrently, the GFRP outer envelope exerted a robust passive confinement pressure that counteracted the transverse tensile strains within the newly cast grout layer. This confinement effectively delayed the shear and compressive degradation of the grout matrix under intense bending moments, maintaining the structural integrity of the tension zone up to the point of ultimate failure. The final shift in failure mode to a predictable, explosive GFRP rupture-completely devoid of premature debonding−confirms that the restored grout matrix successfully sustained the high interfacial shear stresses demanded by the fully utilized composite sheets, validating the profound synergistic efficiency of this dual-material system.

4.4. Steel Load and Strain Relationship

The strain of steel reinforcement in this study was measured using a strain gauge attached directly to the reinforcement. Data were recorded through a data acquisition system in real time, ensuring an accurate correlation between external loads and the reinforcement's strain response. The yield strain values (ε_y) of the D13 and $\varphi 8$ reinforcement bars, obtained from separate tensile tests, were $1589 \mu\varepsilon$ and $1879 \mu\varepsilon$, respectively. These values serve as references for evaluating reinforcement behavior in composite beams.

Analysis of the strain-load curve (Fig. 5) and experimental data (Table 3) showed that the NB control beam exhibited a linear response until it reached the melting point. The NB beam attained an average melting load of 27.37 kN at an average melting strain of 1772.67 $\mu\varepsilon$. The melting strain exceeded the melting stress threshold of the D13 reinforcement material by $1589 \mu\varepsilon$, indicating effective

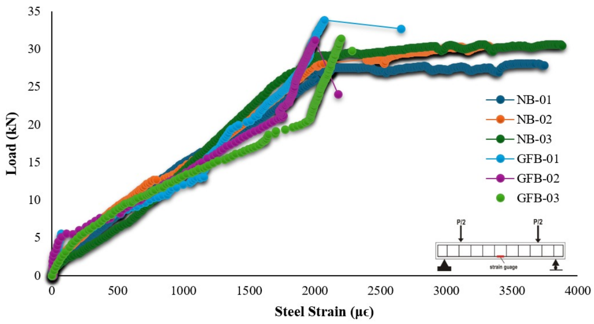

Fig. 5. Steel Load-Strain Relationship Graph.

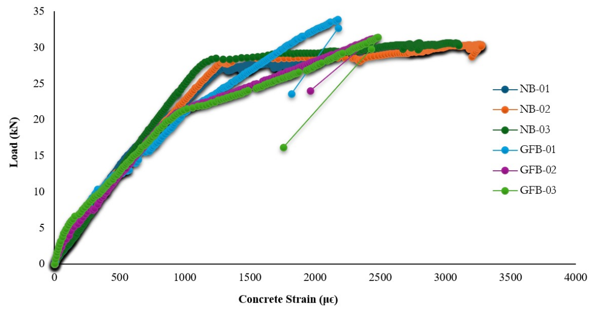

Fig. 6. Concrete Load-Strain Relationship Graph.

composite action between the concrete and the reinforcement, which delays the onset of local melting. This phenomenon aligns with the findings of Dang et al. (2020) [23] and Elkafrawy et al. (2024) [8], who demonstrated that the composite effect increases load capacity before melting due to a more uniform stress distribution. After the melting point, the strain-load curve of the NB beam transitions to elastoplastic behavior, reaching an average ultimate load of 31.24 kN at an ultimate strain of 2813.67$\mu\varepsilon$. This reflects the redistribution of internal stresses and decreased flexural rigidity-a failure mechanism typical of conventional reinforced concrete members [24].

GFRP reinforcement significantly influences the steel strain response in GFB rehabilitation beams. GFB beams achieve an average melting load of 24.04 kN at a melting strain of 1798.33$\mu\varepsilon$. The reduction in the GFB melting load is likely due to the redistribution of the moment to the GFRP layer, which decreases the direct load on the steel reinforcement and affects the bond between the reinforcement and concrete. Importantly, GFB beams attain an average ultimate load of 34.64 kN , representing a substantial increase of 10.87% compared to NB beams. The higher melting strain of GFB(1798.33 $\mu\varepsilon$) relative to NB indicates an enhanced initial deformation capacity. These findings regarding ultimate capacity enhancement align with studies by Karzad et al. (2019) [24], which demonstrate that GFRP reinforcement increases the ultimate moment and extends the plastic phase through an external flexural holding mechanism. The average melting strain of GFB reinforcement (1798.33 $\mu\varepsilon$), which is slightly below the mechanical test value for reinforcement $\varphi 8$(1879 $\mu\varepsilon$), confirms that standard test material parameters remain applicable in the design of GFRP-reinforced beams.

4.5. Concrete Load and Strain Relationship

The measurement of concrete strain in this study was conducted using strain gauges installed in the block pressure zone. Data were recorded in real time using a data acquisition system, ensuring an accurate correlation between load and strain response. As shown in Table 2 and the graph in Fig. 6, the control beam (NB) exhibits a linear-elastic response until it reaches the melting point. The average melt load on the NB beam is 27.37 kN , with the average concrete strain at this point being 1159.33$\mu\varepsilon$, indicating that the concrete can withstand high loads before the steel reinforcement reaches melting. The NB beam then achieves an average ultimate load of 31.24 kN, with an average concrete ultimate strain of 2821.00$\mu\varepsilon$. This ultimate strain value is consistent with previous research, demonstrating that concrete can sustain significant strain before failure [15]. This response indicates that the NB beam has excellent flexural performance, bearing the load until it reaches the ultimate condition before severe structural damage occurs. Although the average ultimate strain value of 2821.00 $\mu\varepsilon$ is slightly below the planned ultimate strain value of 3000$\mu\varepsilon$, it indicates that the beam has good resistance to deformation and reliable concrete quality. This aligns with findings by Maranan et al. (2015) [25], emphasizing the importance of concrete quality in resisting post-crack deformation.

Reinforcement with GFRP on GFB beams significantly alters the strain response of concrete, as shown in Table 2. The average melt load on GFB beams is 24.04 kN , with an average concrete strain at melt of 1048.33 $\mu\varepsilon$. Although the melt load is slightly lower than that of NB beams, the strain value of the melted concrete is also lower. This is due to the additional rigidity provided by the GFRP layer, which binds the sides of the beams and limits the deformation and movement of the concrete during the elastic stage [20]. Most importantly, the average ultimate load of GFB beams increased to 34.64 kN , representing a 10.87 % increase compared to NB beams. This increase in strength confirms the effectiveness of GFRP reinforcement in enhancing the tensile capacity of the beams through a more uniform load distribution mechanism. GFB beams achieve an average concrete ultimate strain of 2391.00 $\mu\varepsilon$, indicating that GFRP reinforcement increases strength and contributes to an overall improvement in ductility. These findings align with previous research demonstrating that adding a GFRP layer to damaged reinforced concrete blocks can increase strength and rigidity, even when the initial stiffness decreases due to structural damage.

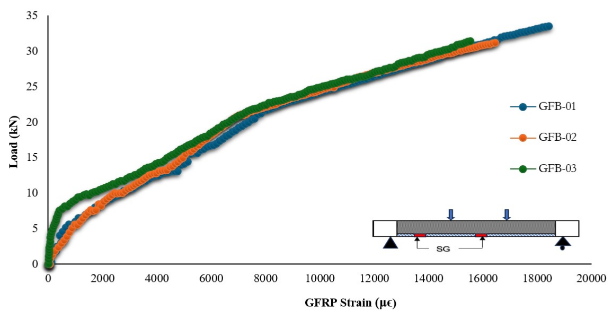

Fig. 7. GFRP Load-Strain Relationship Graph.

4.6. GFRP Load and Strain Relationship

GFRP strain measurements were conducted using strain gauges installed on the surface of composite sheets. These measurements aimed to evaluate the response of GFRP to applied loads, a critical aspect of the reinforcing mechanism. Strain data were recorded in real time using a data logger and analyzed to determine the relationship between external load and strain response. Fig. 7 presents all three GFRP (GFB) reinforced beam specimens, which exhibited consistent responses. Specimen GFB-01 achieved an ultimate load (Pu) of 36.35 kN with an ultimate GFRP strain of $18,532\mu\varepsilon$. GFB-02 reached a Pu of 33.69 kN with a GFRP strain of $16,643\mu\varepsilon$, while GFB-03 attained a Pu of 33.89 kN with a GFRP strain of $15,672\ \mu\varepsilon$. These results demonstrate that GFRP reinforcement significantly enhances the ultimate capacity of the beam, enabling it to withstand higher loads.

Optimizing the amount of GFRP reinforcement is essential to balance flexural strength enhancement and structural ductility, as excessive installation can lead to overstiffening and trigger premature shear failure [26]. In this study, the GFB specimens effectively resisted bending deformation without such premature failure, supported by a critical observation regarding the failure sequence: the internal steel reinforcement reached its actual yield point (average $\varepsilon_s = 1798.33\ \mu\varepsilon$) prior to the GFRP rupture (average $\varepsilon_f = 17,102\ \mu\varepsilon$). This sequence (Steel Yielding → GFRP Rupture) confirms that the designed reinforcement provides a desirable ductile-to-brittle transitional behavior. By ensuring that yielding occurs before the ultimate capacity is reached, the rehabilitation system provides sufficient structural warning before total collapse, which is vital for seismic resilience and safety design.

4.7. Analysis of Crack Patterns and Failure Mechanisms of GFRP Reinforced Concrete Beams

Figure 8 shows the crack pattern on the control reinforced concrete (NB) block, which visually confirms that the dominant failure mechanism is bending cracking. Observations during the test showed that the first cracks appeared in the tensile zone, characterized by a vertical pattern that propagated from the bottom fiber to the neutral axis of the cross-section. This phenomenon is a direct consequence of the inability of concrete materials to withstand tensile stresses that exceed their tensile strength. In the early stages, cracks form in the area of maximum bending momentum, about 1/3 of the middle span, and develop progressively towards the compressive fibers as the load increases. This propagation process continues until it reaches peak load, where the maximum load capacity is reached. Even though deflection continues to increase significantly, the structure can withstand loads characteristic of ductile failure. These findings are supported by the study of Elkafrawy et al. (2024) [8], which demonstrated the effectiveness of FRP external reinforcement in delaying the initiation of cracks and increasing load capacity before collapse. Further, [17, 27] affirm that FRP reinforcement systems significantly increase resistance to initial crack formation and prolong the plastic phase before collapse, directly contributing to the structure's overall ductility.

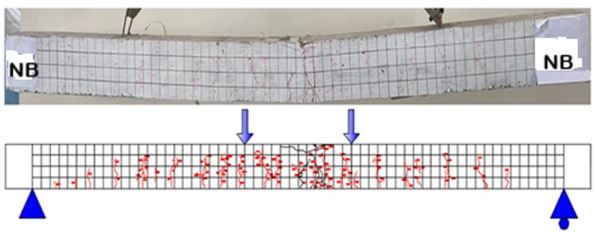

Fig. 8. Concrete beam crack pattern NB.

Fig. 9 visually illustrates the crack pattern in beams reinforced with Glass FiberReinforced Polymer (GFRP) sheets. The observations reveal a more complex failure mechanism than non-reinforced (NB) beams. Although bending cracks remain the primary failure mode, the GFRP layer alters the failure pattern. The first bending crack in the GFRPreinforced beam (GFB) was recorded at a load of 5.53 kN, higher than the 3.4 kN observed in the NB beam, indicating an increase in initial strength due to the added lateral stiffness of the composite system. As the load increases, this initial bending crack propagates vertically; however, at approximately 21.25 kN , oblique cracks begin to appear near the ends of the GFRP strip as the tensile reinforcement starts to yield. These skewed cracks indicate localized shear stress concentration in the area. This phenomenon has been reported by [26] as a potential indicator of premature shear failure if the reinforcement design is suboptimal. In this case, however, shear failure does not occur. Final failure happens at an ultimate load of 33.85 kN , after the bending crack has propagated beyond three-quarters of the span length. At this stage, significant plastic deformation in both the reinforcement and concrete causes the strain in the GFRP layer to reach a maximum of $18,532\ \mu\varepsilon$ in the GFB-01 specimen, which is close to the ultimate strain capacity of the GFRP material (2.5%). Consequently, interfacial debonding occurs between the GFRP and concrete, characterized by a loud popping sound and white streaks extending vertically from the tensile zone to the compressive block area. A total of 20 cracks were observed on the GFB beam, indicating that cracking had spread across nearly the entire beam cross-section.

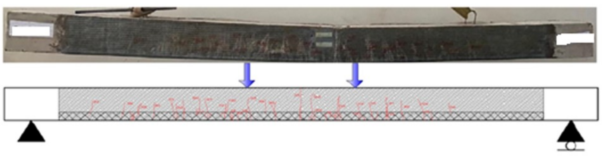

Fig. 9. GFB concrete beam cracking pattern.

Fig. 10 illustrates the progressive failure evolution observed in the GFRP-strengthened beams. Experimental observations revealed that the failure process was preceded by several identifiable damage indicators, including the gradual propagation of flexural cracks, the formation of localized oblique cracks near the GFRP termination zones, increasing concrete cracking sounds, and the development of microcracking around the critical flexural regions. Microcracking became noticeable at approximately 20.6 kN and progressively intensified as the applied load increased, leading to localized stiffness degradation and stress concentration near the composite interface. At approximately 30.3 kN , audible cracking activity became more frequent, indicating progressive internal damage accumulation prior to ultimate failure. Final debonding and GFRP rupture occurred at approximately 33.85 kN after substantial crack propagation and large deformation had already developed within the beam system.

Although GFRP materials exhibit predominantly brittle linear-elastic behavior up to rupture, the observed structural response in the present study was not characterized by instantaneous catastrophic collapse without warning. Instead, the failure progression remained observable and mechanically traceable through progressive cracking patterns, increasing deformation, and localized interface deterioration prior to final rupture. Therefore, the term "failure predictability" used in this study refers to the ability to identify consistent and progressive pre-failure indicators during loading, rather than implying ductile yielding behavior similar to conventional steel-reinforced concrete systems [27, 28]. Similar observations have been reported in previous studies, where externally bonded FRP systems produced identifiable crack evolution and stable failure progression before ultimate debonding or rupture [17, 20].

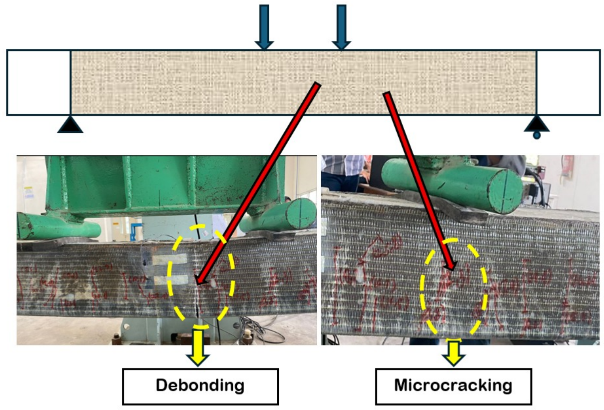

Fig. 10. GFB beam collapse mode.

This process confirms that the ultimate failure of the GFB beam resulted from progressive damage accumulation, beginning with macrocracking, followed by microstructural degradation and localized interface deterioration prior to final debonding. The observed behavior demonstrates that the failure mechanism was not governed solely by material rupture, but rather by complex interactions among the existing concrete substrate, repair grout, epoxy adhesive, and externally bonded GFRP system. Therefore, the integrity of the composite interfaces, particularly the bond between the original concrete and the non-shrink grout layer, played a critical role in ensuring effective stress transfer throughout the loading process. Premature debonding at the repair interface could significantly reduce the strengthening efficiency and alter the intended flexural failure mechanism of the rehabilitated beam [17, 27].

Experimental observations revealed no visible separation or delamination between the original concrete substrate and the Sikagrout 215 repair layer up to ultimate failure, indicating satisfactory interface compatibility and effective composite action within the rehabilitated system. The relatively compatible modulus of elasticity between the substrate concrete (approximately 25 GPa) and the repair grout ($\geq$ 25GPa) likely minimized differential deformation and reduced interfacial stress concentrations under flexural loading. Furthermore, the mechanical surface preparation conducted prior to grout application enhanced the mechanical interlocking mechanism and improved bond continuity between the old and repaired concrete surfaces [21, 23].

The failure mode was governed primarily by progressive flexural cracking followed by localized GFRP debonding near the sheet termination zones, rather than grout delamination from the concrete substrate. This behavior suggests that the concrete-grout interface remained structurally stable and capable of transferring stresses effectively to the externally bonded GFRP system throughout the loading history. Similar findings have been reported by Karimipour and Edalati [17] and Rageh et al. [20], who emphasized that the effectiveness of FRP rehabilitation systems strongly depends on maintaining interface integrity and compatible deformation behavior between repair materials and the existing structural substrate. In addition, previous studies [16, 24] reported that externally bonded fiber composites not only enhance tensile resistance but also delay concrete deterioration through confinement and stress redistribution effects, thereby producing a more controlled and predictable failure mechanism. Overall, the crack patterns and failure characteristics observed in the GFB specimens confirm that the integrated rehabilitation strategy successfully restored structural capacity while maintaining stable composite action without premature interface failure. Nevertheless, direct interface bond characterization tests, such as slant shear or pull-off tests, were beyond the scope of the present investigation. Therefore, further studies incorporating dedicated interface characterization and long-term durability evaluation are recommended to quantify the bond performance of the integrated grout-GFRP rehabilitation system more comprehensively.

Another limitation of the present study is the absence of additional comparative control groups consisting of specimens rehabilitated solely with repair grout or exclusively with externally bonded GFRP without prior geometric restoration. The primary objective of this investigation was to evaluate the overall structural effectiveness of an integrated rehabilitation strategy combining non-shrink grout restoration and external GFRP strengthening under mechanically representative deterioration conditions, rather than to isolate the individual contribution of each rehabilitation component. Nevertheless, the inclusion of grout-only and GFRP-only specimens would provide a more comprehensive understanding of the interaction mechanisms and potential synergistic effects between geometric restoration and external composite strengthening. Previous studies have shown that repair grout primarily contributes to restoring section geometry and local stiffness, whereas FRP systems predominantly enhance tensile resistance and flexural capacity [5, 17, 20]. Therefore, future experimental investigations incorporating additional control groups are recommended to quantify the relative contribution of each rehabilitation component and to establish the extent of composite synergy within integrated repair systems more rigorously.

5. Conclusions

- The integrated rehabilitation strategy, combining high-strength non-shrink grout and externally bonded GFRP, successfully restores and enhances the structural integrity of corrosion-damaged RC beams.
- The rehabilitated beams (GFB) achieved an average ultimate load of 34.64 kN , which is 10.87% higher than the sound control beams (31.24 kN), despite the initial severe section loss.
- While the GFRP layer resulted in a slightly lower ultimate concrete strain $(2391\mu\varepsilon)$ compared to control beams $(2821\mu\varepsilon)$, the specimens exhibited superior structural resilience, enhanced post-yield deformation capacity, and a more progressive and mechanically traceable failure mechanism.
- GFRP strain measurements (up to $18,532\mu\varepsilon$) confirmed high material utilization, with the failure mode shifting from ductile flexural failure to a controlled GFRP rupture without premature shear failure.
- The experimental observations confirmed satisfactory composite action between the existing concrete substrate, repair grout, epoxy adhesive, and externally bonded GFRP system, with no premature grout-interface delamination observed prior to ultimate failure.
- The dual-phase rehabilitation approach (grout restoration followed by GFRP strengthening) provides an effective, evidence-based solution for extending the service life of saltdamaged or aging infrastructure.

Acknowledgements

The authors express their sincere gratitude for the self-funding that supported the entire research process through to its completion. This financial commitment demonstrates their full dedication to the researched topic.

References

[1] Y. Zhou, Y. Zheng, J. Pan, L. Sui, F. Xing, H. Sun, and P. Li, (2019) *"Experimental investigations on corrosion resistance of innovative steel-FRP composite bars using X-ray microcomputed tomography"* **Composites Part B: Engineering *161***: 272–284. DOI: 10.1016/j.compositesb.2018.10.069.

[2] G. G. Triantafyllou, T. C. Rousakis, and A. I. Karabinis, (2017) *"Analytical assessment of the bearing capacity of RC beams with corroded steel bars beyond concrete cover cracking"* **Composites Part B: Engineering *119***: 132–140. DOI: 10.1016/j.compositesb.2017.03.036.

[3] L. Dai, P. Chen, X. Luo, L. Wang, and J. Zhang, (2024) *"Prediction of corrosion-induced retraction slip of prestressing strand in pre-tensioned concrete beams"* **Structure and Infrastructure Engineering *20***(11): 1778–1789. DOI: 10.1080/15732479.2023.2165117.

[4] D. M. Frangopol and M. Liu, (2007) *"Maintenance and management of civil infrastructure based on condition, safety, optimization, and life-cycle cost"* **Structure and Infrastructure Engineering *3***(1): 29–41. DOI: 10.1080/15732470500253164.

[5] Y. Mugahed Amran, R. Alyousef, R. S. Rashid, H. Alabduljabbar, and C.-C. Hung, (2018) *"Properties and applications of FRP in strengthening RC structures: A review"* **Structures *16***: 208–238. DOI: 10.1016/j.istruc.2018.09.008.

[6] J. Tatar and S. Milev, (2021) *"Durability of externally bonded fiber-reinforced polymer composites in concrete structures: a critical review"* **Polymers *13***(5): 765. DOI: 10.3390/polym13050765.

[7] A. Diniță, R. G. Ripeanu, C. N. Ilincă, D. Cursaru, D. Matei, R. I. Naim, M. Tănase, and A. I. Portoacă, (2023) *"Advancements in fiber-reinforced polymer composites: a comprehensive analysis"* **Polymers *16***(1): 2. DOI: 10.3390/polym16010002.

[8] M. Elkafrawy, P. Gowrishankar, N. G. Aswad, A. Alashkar, A. Khalil, M. AlHamaydeh, and R. Hawileh, (2024) *"GFRP-reinforced concrete columns: state-of-the-art, behavior, and research needs"* **Buildings *14***(10): 3131. DOI: 10.3390/buildings14103131.

[9] M. Alhusban, M. Alhusban, and A. A. Alkhawaldeh, (2023) *"The Efficiency of Using Machine Learning Techniques in Fiber-Reinforced-Polymer Applications in Structural Engineering"* **Sustainability *16***(1): 11. DOI: 10.3390/su16010011.

[10] R. E. Melchers, C. Q. Li, and W. Lawanwisut, (2006) *"Modelling deterioration of structural behaviour of reinforced concrete beams under saline environment corrosion"* **Magazine of Concrete Research *58***(9): 575–587. DOI: 10.1680/macr.2006.58.9.575.

[11] D. Coronelli and P. Gambarova, (2004) *"Structural assessment of corroded reinforced concrete beams: modeling guidelines"* **Journal of Structural Engineering *130***(8): 1214–1224. DOI: 10.1061/(ASCE)0733-9445(2004)130:8(1214).

[12] S. Barbhuiya, B. B. Das, and F. Kanavaris, (2024) *"A review of fracture propagation in concrete: fundamentals, experimental techniques, modelling and applications"* **Magazine of Concrete Research *76***(10): 482–514. DOI: 10.1680/jmacr.23.00143.

[13] H. Lee, H. Jang, and W. Chung, (2019) *"Effect of recycled concrete on the flexural behavior of concrete-filled FRP tubes"* **International Journal of Concrete Structures and Materials *13***(1): 12. DOI: 10.1186/s40069-018-0318-8.

[14] A. Cohades, C. Branfoot, S. Rae, I. Bond, and V. Michaud, (2018) *"Progress in self-healing fiber-reinforced polymer composites"* **Advanced Materials Interfaces *5***(17): 1800177. DOI: 10.1002/admi.201800177.

[15] P. W. R. Beaumont, (2020) *"The structural integrity of composite materials and long-life implementation of composite structures"* **Applied Composite Materials *27***(5): 449–478. DOI: 10.1007/s10443-020-09822-6.

[16] C. Miàs, L. Torres, M. Guadagnini, and A. Turon, (2015) *"Short and long-term cracking behaviour of GFRP reinforced concrete beams"* **Composites Part B: Engineering *77***: 223–231. DOI: 10.1016/j.compositesb.2015.03.024.

[17] A. Karimipour and M. Edalati, (2021) *"Retrofitting of the corroded reinforced concrete columns with CFRP and GFRP fabrics under different corrosion levels"* **Engineering Structures *228***: 111523. DOI: 10.1016/j.engstruct.2020.111523.

[18] S. A. Khan, (2024) *"Enhancing the mechanical properties of fibre-reinforced concrete through sustainable mix design: effects of fibre type and dose"* **Discover Civil Engineering *1***(1): 88. DOI: 10.1007/s44290-024-00087-7.

[19] J. Johnson and S. Eswari, (2025) *"Flexural and ductile characteristics of glass fibre reinforced polymer bar-reinforced concrete incorporating basalt fibres of varied lengths"* **Innovative Infrastructure Solutions *10***(9): 399. DOI: 10.1007/s41062-025-02204-6.

[20] B. O. Rageh, M. A. El-Mandouh, A. H. Elmasry, and M. M. Attia, (2022) *"Flexural behavior of RC beams strengthened with GFRP laminate and retrofitting with novelty of adhesive material"* **Buildings *12***(9): 1444. DOI: 10.3390/buildings12091444.

[21] C. Mensah, Z. Wang, A. O. Bonsu, and W. Liang, (2020) *"Effect of different bond parameters on the mechanical properties of FRP and concrete interface"* **Polymers *12***(11): 2466. DOI: 10.3390/polym12112466.

[22] H. Fergani, M. Di Benedetti, C. Miàs Oller, C. Lynsdale, and M. Guadagnini, (2018) *"Durability and degradation mechanisms of GFRP reinforcement subjected to severe environments and sustained stress"* **Construction and Building Materials *170***: 637–648. DOI: 10.1016/j.conbuildmat.2018.03.092.

[23] Z. Dang, P. Feng, J.-Q. Yang, and Q. Zhang, (2020) *"Axial compressive behavior of engineered cementitious composite confined by fiber-reinforced polymer"* **Composite Structures *243***: 112191. DOI: 10.1016/j.compstruct.2020.112191.

[24] A. S. Karzad, M. Leblouba, S. A. Toubat, and M. Maalej, (2019) *"Repair and strengthening of shear-deficient reinforced concrete beams using Carbon Fiber Reinforced Polymer"* **Composite Structures *223***: 110963. DOI: 10.1016/j.compstruct.2019.110963.

[25] G. Maranan, A. Manalo, B. Benmokrane, W. Karunasena, and P. Mendis, (2015) *"Evaluation of the flexural strength and serviceability of geopolymer concrete beams reinforced with glass-fibre-reinforced polymer (Gfrp) bars"* **Engineering Structures *101***: 529–541. DOI: 10.1016/j.engstruct.2015.08.003.

[26] M. Goldston, A. Remennikov, and M. N. Sheikh, (2017) *"Flexural behaviour of GFRP reinforced high strength and ultra high strength concrete beams"* **Construction and Building Materials *131***: 606–617. DOI: 10.1016/j.conbuildmat.2016.11.094.

[27] M. K. Askar, A. F. Hassan, and Y. S. Al-Kamaki, (2022) *"Flexural and shear strengthening of reinforced concrete beams using FRP composites: A state of the art"* **Case Studies in Construction Materials *17***: e01189. DOI: 10.1016/j.cscm.2022.e01189.

[28] J. D. Ortiz, S. S. Khedmatgozar Dolati, P. Malla, A. Nanni, and A. Mehrabi, (2023) *"Frp-reinforced/strengthened concrete: state-of-the-art review on durability and mechanical effects"* **Materials *16***(5): 1990. DOI: 10.3390/ma16051990.